

Design and Performance Analysis of Hydrokinetic Turbine with Aerodynamic Stall Model



Mahendra Kumar Gupta and P. M. V. Subbarao

Nomenclature

A	Rotor swept area (m^2)
a	Induced axial flow (dimensionless)
a'	Induced tangential flow (dimensionless)
B	Number of blades (dimensionless)
C_d	Coefficient of drag (dimensionless)
C_l	Coefficient of lift (dimensionless)
C_p	Rotor power coefficient (dimensionless)
C_t	Coefficient of thrust (dimensionless)
c	Blade section chord length (m)
F	Prandtl's tip loss correction factor (dimensionless)
k	Blade aspect ratio (dimensionless)
N	Number of blade elements (dimensionless)
P	Rotor power (W)
R	Radius of a rotor (m)
Re	Reynolds Number (dimensionless)
r	Radial position of blade element (m)
U_a	Axial fluid velocity (m/s)
U_t	Tangential fluid velocity (m/s)
V_o	Free stream fluid velocity (m/s)
V_{rel}	Relative velocity (m/s)
α	Angles of attack (deg)
α_s	Stall angle (deg)
λ	Tip speed ratio (dimensionless)
Ω	Rotational speed of a rotor (rad/s)

M. K. Gupta (✉) · P. M. V. Subbarao

Department of Mechanical Engineering, Indian Institute of Technology Delhi, New Delhi 110016, India

\emptyset	Flow angle (deg)
ρ	Density of the fluid (kg/m^3)
σ	Solidity (dimensionless)
θ	Local pitch angle (degree)
θ_p	Blade pitch angle (degree)
i	i th blade section
j	j th iteration
s	the starting point at stall angle (degree)

1 Introduction

Conventional hydropower plant requires a high head of water to drive turbines, but what if, there are zero head or little head of water. A feasible solution to this lies in hydrokinetic turbines (HKT). HKT systems are electromechanical energy converters that convert the kinetic energy of river streams, tidal currents and human-made water channels into other usable forms of energy.

1.1 Hydrokinetic Turbine's Principle

The energy conversion principle of HKT and wind turbines is the same. So for the study of free flow hydrokinetic turbines, the corresponding parameters of wind turbines can be used from Khan et al. [1]. Comprehensive reviews on HKT including detailed fundamental studies and turbine classification can be found in Khan and Iqbal [2] and Khan et al. [3].

The amount of hydrokinetic power available for extraction depends on the free stream fluid velocity (V_o), rotor swept area (A) and density of the fluid (ρ). The power coefficient (C_p) determines the performance of HKT as expressed in Eq. 1, Swenson [4]. The typical overall efficiency for a hydrokinetic turbine with low-mechanical losses is approximately 30%, Tiago [5]. The performance of HKT depends primarily on these design parameters, tip speed ratio (TSR), solidity (σ) and blade pitch angle (θ_p). The TSR (λ) expressed in Eq. 2 is defined as the ratio of the blade tip speed to the fluid velocity (V_o). The solidity is related to the radius (R), blade chord length (c), and some blades (B), and it is the ratio of the planform area of the blades to the swept area as expressed in Eq. 3.

Generally, a low-solidity axial flow turbine turns at a higher TSR than a high solidity turbine, results in higher rotational speed for the same diameter and current speed. However, solidity should be kept around 30% to produce enough starting torque, as demonstrated by the Brazilian and Australian experiences, Swenson [4], Tiago [5].

Hydrokinetic energy converters can be divided into lift based and drag based machines. The maximum power coefficient, which can be achieved in a drag based device, is 0.29, which is significantly lower than the Betz limit of 0.59, Bahaj et al. [6]. Hence, all modern hydrokinetic turbines are being designed on lift principles, using airfoils which should have a significant lift to drag ratio to achieve a maximum coefficient of performance (C_p). Here, author focuses on horizontal axis hydrokinetic turbine (HAHkT) among other HKT because it can self-start in lower flow velocities, and the horizontal axis of rotation allows each blade to produce a continuous torque throughout one rotation, outputting a smooth and constant power, Batten et al. [7].

$$C_p = \frac{P}{(1/2)\rho A \mathbf{V}_0^3} = \frac{\text{Rotor Power}}{\text{Power in the water current}} \quad (1)$$

$$\lambda = \frac{\Omega R}{\mathbf{V}_0} \quad (2)$$

$$\sigma = \frac{Bc}{2\pi R} \quad (3)$$

For predicting the performance, and designing of HAHkT, the most employed method is the blade element momentum theory (BEM), Bahaj and Myers [8], Batten [9], and Massouh and Dobrev [10]. The starting point for a BEM model is the knowledge of the reliable two-dimensional (2D) aerodynamic coefficient; lift (C_l) and drag (C_d), but these coefficients are often available only for small angles of attack (α) (attached regime), while a large range of α (stalled regime) appears on the blade element of the rotor when HAHkT operates at high speed.

To overcome this problem of non-availability of C_l and C_d in the stalled regime of the blade element, the mathematical models for estimation of lift and drag coefficients in this region have been proposed by Viterna and Corrigan (VC), Viterna and Corrigan [11]. Prandtl's tip loss correction factor (F) to account the finite-size effect of a rotor blade, Manwell and McGowan [12] and the VC model is incorporated with original BEM model so that improved BEM model can predict rotor performance correctly for a wide range of α .

1.2 Blade Design and Modeling

In BEM theory, the rotor blade is divided into some elemental sections along the span, and both the linear and angular momentum changes of flowing water through the rotor disk are balanced with the axial force and torque generated on the rotor blades, respectively, Manwell and McGowan [12].

Figure 1 shows the velocity diagram for the current configuration, where V_{rel} is the relative velocity; the combination of axial fluid velocity (U_a), and tangential fluid velocity due to the rotation (U_t). The angle between chord and rotor plane, between

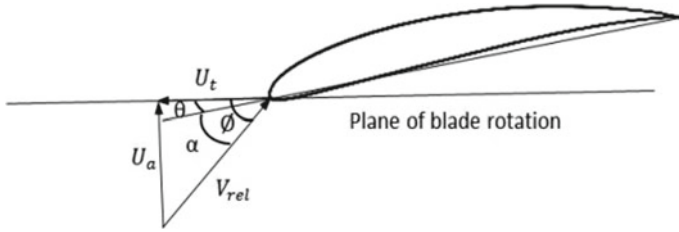


Fig. 1 Velocity diagram for airfoil

the rotor plane and V_{rel} and between chord and V_{rel} are local pitch angle (θ), flow angle (ϕ) and angle of attack (α), respectively.

2 Mathematical Model for the Aerodynamic Characteristics of an Airfoil in Stall Regimes

Comparisons among power curve of different horizontal axis wind turbine (HAWT) have been shown for different aerodynamic models and conclude that VC model predicts close to experimental data, David [13]. The VC model plays an important role in predicting the peak power of a fixed pitch turbine.

In Viterna–Corrigan stall model lifting line theory has been used for prediction of airfoil properties in attached regime only ($\alpha < \alpha_s$), and finite-size effects have been considered by this theory in this VC model. For blade element under the stalled regime ($\alpha > \alpha_s$), Viterna–Corrigan developed the following empirical relations to predict C_l and C_d , depending on the blade aspect ratio (k).

$$C_l = \frac{1}{2}C_{D,max} \sin 2\alpha + A_2 \cos^2 \alpha / \sin \alpha \tag{4}$$

$$C_d = C_{d,max} \sin^2 \alpha + B_2 \cos \alpha \tag{5}$$

where

$$A_2 = \frac{(C_{L,s} - C_{D,max} \sin \alpha_s \cos \alpha_s) \sin \alpha_s}{\cos^2 \alpha_s} \tag{6}$$

$$B_2 = (C_{D,s} - C_{D,max} \sin^2 \alpha_s) / \cos \alpha_s \tag{7}$$

$$C_{D,max} = \begin{cases} 1.11 + 0.018k, & k \leq 50 \\ 2.01 & k > 50 \end{cases} \tag{8}$$

The subscript s denotes the constant at stall angle (α_s). $C_{D,max}$ is the maximum drag coefficient at an angle of attack of 90° .

3 Modified BEM Model

For predicting the performance of low-aspect ratio rotor blade, the original BEM theory can be validated with an experiment in attached regime only. Tests on the NASA Mod-0 100 kW wind turbine indicated that for finite-sized rotor blade operating at higher α , BEM theory was incapable of predicting rotor performance in stalled regime, Viterna and Corrigan [11].

So BEM theory is improved with the inclusion of Prandtl's tip loss correction factor to account for losses due to fluid flow from the pressure side to suction side at the blade's tip, Manwell and McGowan [12] and VC model described above.

In BEM theory, blade is divided into N elements (Fig. 1), and rotor theory is applied to each element to estimate the shape of each element. Due to the presence of rotor, induced axial and tangential flow field at the rotor plane is expressed as a and a' , respectively. At each rotor blade element (r_i), after initialization for $a_{i,1}$ and $a'_{i,1}$, the iterative solution procedure for the j -th iteration is as follows, Manwell and McGowan [12].

$$\tan \vartheta_{i,j} = \frac{1 - a_{i,j}}{(1 + a'_{i,j})\lambda_{r,i}} \quad (9)$$

$$F_{i,j} = \left(\frac{2}{\pi}\right) \cos^{-1} \left[\exp \left(- \left\{ \frac{(B/2)[1 - (r_i/R)]}{(r_i/R) \sin \vartheta_{i,j}} \right\} \right) \right] \quad (10)$$

$$a_{i,j+1} = \frac{1}{(1 + 4F_{i,j} \sin^2 \vartheta_i / (\sigma'_i C_{l,i} \cos \vartheta_i))} \quad (11)$$

$$a'_{i,j+1} = \frac{1}{(4F_{i,j} \cos \vartheta_i / \sigma'_i C_{l,i}) - 1} \quad (12)$$

4 Results and Discussion

4.1 Predicted Aerodynamic Coefficients in the Stalled Regime

Among other airfoils designed specially for HAWT, the S809 airfoil has significant lift-to-drag ratio under an operating range of Re from 10^5 to 10^6 , which also comes

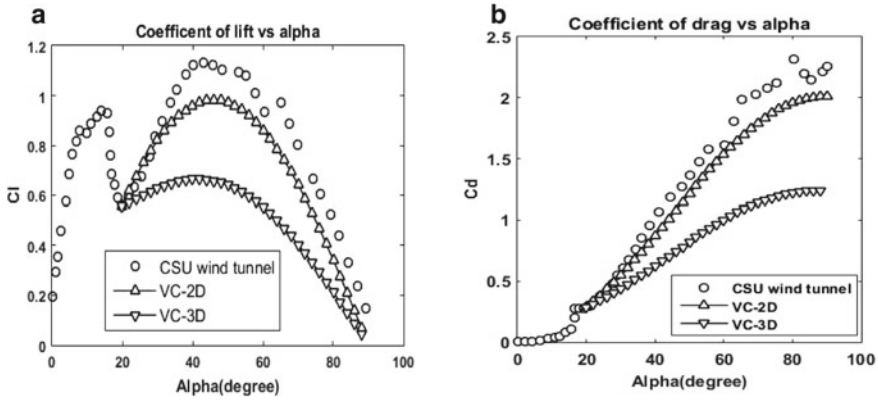


Fig. 2 a, b Measured versus predicted aerodynamic coefficients for S809 at Re 650,000

under our working conditions. This airfoil was designed with an objective of insensitivity toward leading edge (LE) roughness so that the value of the maximum lift coefficient does not decline due to debris over LE of an airfoil, Somers and Dan [14].

For testing the VC model against measured data, the measured aerodynamic data for the whole range of α up to 90° is available only at the Reynolds number of 650,000 (CSU) for S809 airfoil. Martínez et al. [15] showed that predicted 2D data using the VC model is close to measured 2D data if α_s is chosen corresponding to the local $C_{l,min}$ rather than $C_{l,max}$ which was suggested by the original Viterna–Corrigan model.

Many authors found that in the attached regime, the performance of the rotor can be predicted well using 2D aerodynamic coefficient, so 2D and 3D aerodynamic data are predicted using the VC model for stall regime only.

Predicted 2D aerodynamic coefficients are compared with measured data (CSU wind tunnel) in Fig. 2. It can be seen that predicted 2D aerodynamic coefficients in the stall regime using VC-2D ($k > 50$) are close to 2D experimental data as compare to VC-3D (for $k < 50$).

4.2 Rotor Performance Predictions with Modified BEM

The fixed point iterative numerical approach was used in MATLAB to calculate optimized blade profile, and C_p . Blade designed data are shown in Table 1.

Axial induction factor(a) distribution along the blade for pitch angle of 0° , 1° , 3° and 5° are shown in Fig. 3. It can be seen that for pitch angle of zero and one degree and at tip speed ratio (TSR) of 6.28, a is close to Betz limit of $(1/3)$ and results in a maximum coefficient of power (C_p) at this position.

Table 1 Blade designed data

Design parameters	Values
Rated power (W)	800
Nominal water current velocity (m/s)	2
Design TSR (λ)	4
Number of blades	3
Airfoils	S809

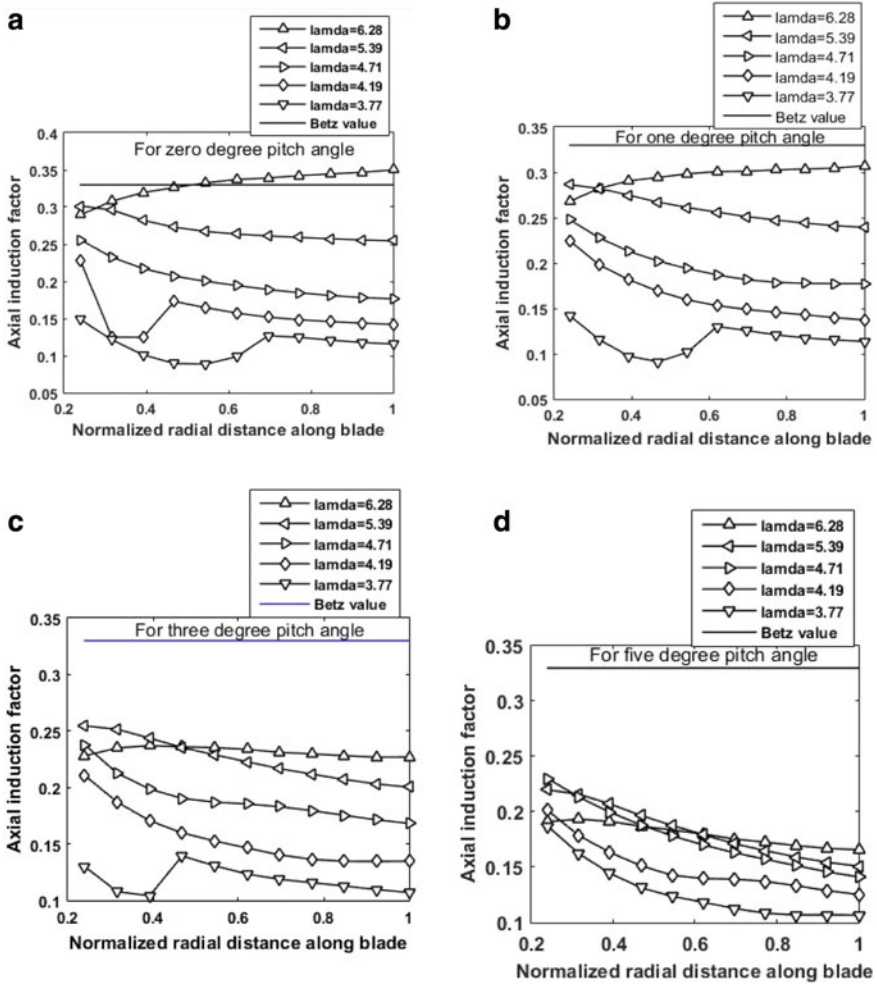


Fig. 3 a–d Axial Induction factor at different-2 TSR along the blade for pitch angle of 0° , 1° , 3° and 5°

Figure 4a has shown tip loss correction factor (F) distribution along the blade. The figure shows as tip speed ratio (TSR) decreases, the effect of tip loss increases at tip considerably. The effect of tip loss covers approximately 30% of the blade.

From the tip, Figure 4b has shown axial induction factor for pitch angle of 1° with and without considering F . It also indicates that from root to 70% of the blade axial induction factor is same along the blade.

Figure 5 shows the coefficient of power (C_p) versus tip speed ratio (λ) for the pitch angle of 0° , 1° , 3° and 5° . For zero degree and one-degree pitch angle, C_p is almost same and maximum (0.51) at the same TSR of 6.28. For lower TSR, C_p increases as pitch angle increases because axial induction factor and C_l increases correspondingly,

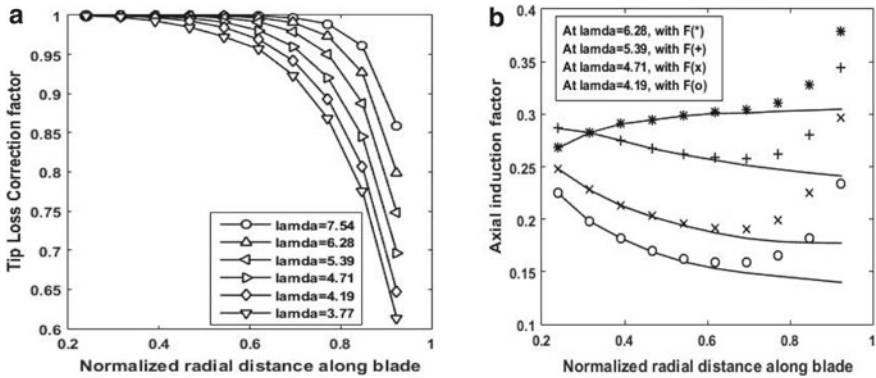


Fig. 4 a Tip loss correction factor at various λ , b Axial Induction factor at various λ with and without F

Fig. 5 Coefficient of power at various pitch angle versus TSR

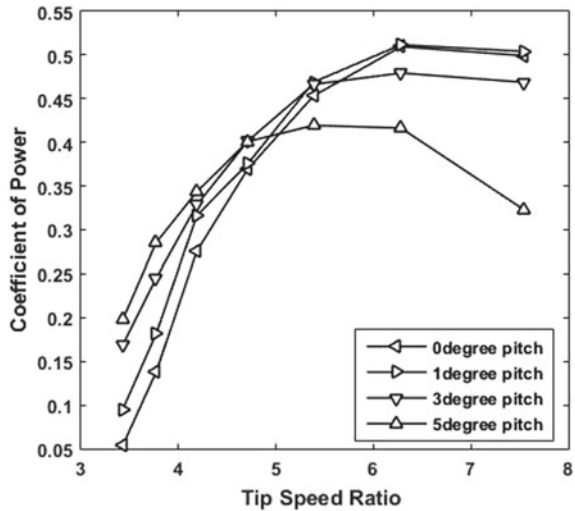
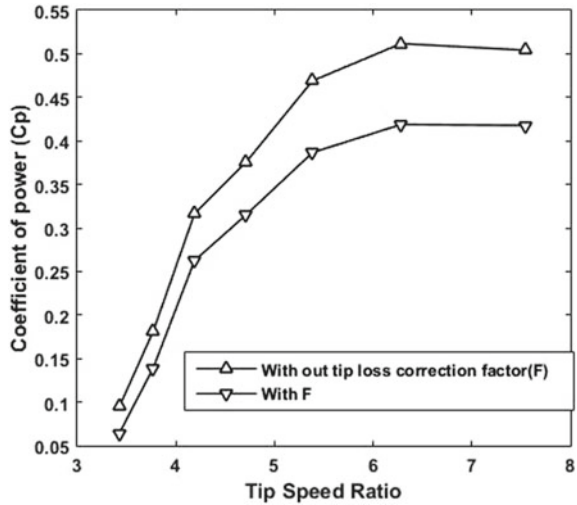


Fig. 6 Comparison of power versus TSR considering F for 1-degree of pitch angle only



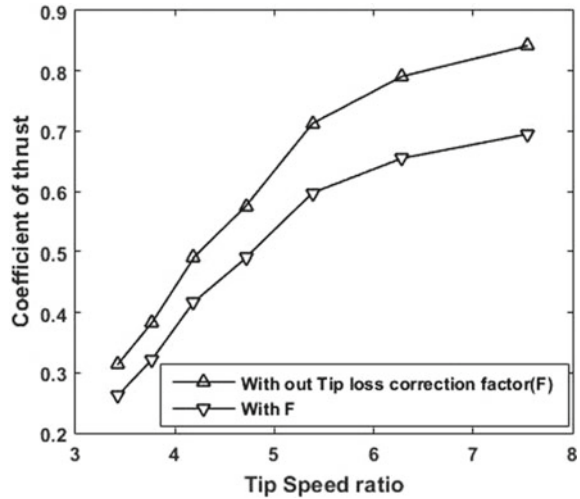
while for higher TSR axial induction factor and C_l decreases shown in Fig. 3, results in a decrement in C_p as pitch angle increases Fig. 5.

Figures 6 and 7 show C_p versus TSR and Coefficient of thrust (C_t) versus TSR for pitch angle of 1-degree considering tip loss correction factor. It can be seen that C_p is 0.42 almost same at $\lambda = 6.28$. C_t increases as TSR increases, but the rate of growth decrease.

5 Conclusions

It has been shown that predicted 2D aerodynamic coefficients in the stall regime using VC-2D ($k > 50$) are close to 2D experimental data as compare to VC-3D (for $k < 50$). It is found that maximum $C_{p,max}$ is 0.50 at optimum λ_{opt} of 6.3 for pitch angle of one degree. With Prandtl's tip loss correction factor (F), it was showed that thirty percent of the blades from the blade's tip is affected due to fluid flow from the pressure side to the suction side, and the effect is significantly higher at large TSR (Figs. 6 and 7).

Fig. 7 Comparison of C_t versus TSR considering F for 1-degree of pitch angle only



Acknowledgements The author wishes to thank his colleagues and supervisor for his invaluable guidance.

References

1. Khan, M. J., Iqbal, M. T., & Quaicoe, J. E. (2008). River current energy conversion systems: Progress, prospects and challenges. *Renewable and Sustainable Energy Reviews*, 12(8), 2177–2193.
2. Khan, M. J., Iqbal, M. T., & Quaicoe, J. E. (2006). *A technology review and simulation-based performance analysis of river current turbine systems*. Ottawa: IEEE CCECE/CCGEI.
3. Khan, M. J., Bhuyan, G., Iqbal, M. T., & Quaicoe, J. E. (2009). Hydrokinetic energy conversion systems and assessment of horizontal and vertical axis turbines for river and tidal applications: A technology status review. *Applied Energy*, 86(10), 1823–1835.
4. Swenson, W. J. (1999). *The evaluation of an axial flow, lift type turbine for harnessing the kinetic energy in the tidal flow*. Darwin, Australia: Australian Universities Power Engineering Conference AUPEC.
5. Tiago, G. L. (2003). *The state of the art of hydrokinetic power in Brazil*. Waterpower XIII, Buffalo New York.
6. Bahaj, A. S., & Myers, L. E. (2003). Fundamentals applicable to the utilization of marine current turbines for energy production. *Renewable Energy*, 28, 2205–2211.
7. Batten, W. M. J., Bahaj, A. S., Molland, A. F., & Chaplin, J. R. (2006). Hydrodynamics of marine current turbines. *Renewable Energy*, 31(2), 249–255.
8. Bahaj, A. S., & Myers, L. E. (2006). Power output performance characteristics of a horizontal axis marine current turbine. *Renewable Energy*, 31, 197–208.
9. Batten, W. M. J., Bahaj, A. S., Molland, A. F., & Chaplin, J. R. (2008). The prediction of hydrodynamics of marine current turbines. *Renewable Energy*, 33, 1085–1096.
10. Massouh, F., & Dobrev, I. (2007). Exploration of the vortex wake behind of wind turbine rotor. *J Phys Conf Ser*, 75, 1–9.

11. Viterna, L. A., & Corrigan, R. D. (1981). Fixed pitch rotor performance of large horizontal axis wind turbines. In *DOE/NASA Workshop on Large Horizontal Axis Wind Turbines*, Cleveland, OH (pp. 69–85).
12. Manwell, J. F., & McGowan, J. G. (2002). *Wind energy explained: Theory, design and application*. New York: John Wiley and Sons.
13. David, A., & Spera (2009). *Wind turbine technology: Fundamental concepts in wind turbine engineering*. New York: ASME.
14. Somers, D. M. (1997). *Design and experimental results for the S809 airfoil*. Airfoils, Inc.
15. Martínez, J., et al. (2005). An improved BEM model for the power curve prediction of stall-regulated wind turbines. *Wind Energy*, 8, 385–402.